High-resolution mapping of infraslow cortical brain activity enabled by graphene microtransistors

Eduard Masvidal-Codina[1], Xavi Illa[2,1], Miguel Dasilva[3], Andrea Bonaccini Calia[4], Tanja Dragojević[5], Ernesto E. Vidal-Rosas[5], Elisabet Prats-Alfonso[2,1], Javier Martínez-Aguilar[1,2], Jose M. De la Cruz Sanchez[4], Ramon Garcia-Cortadella[4], Philippe Godignon[1], Gemma Rius[1], Alessandra Camassa[3], Elena Del Corro[4], Jessica Bousquet[4], Clement Hébert[4], Turgut Durduran[5,6], Rosa Villa[1,2], Maria V Sanchez-Vives[3,6], Jose A Garrido[4,6]* and Anton Guimerà-Brunet[1,2]*

1 Institut de Microelectrònica de Barcelona, IMB-CNM (CSIC), Esfera UAB, Bellaterra, Spain

2 Centro de Investigación Biomédica en Red en Bioingeniería, Biomateriales y Nanomedicina (CIBER-BBN), Madrid, Spain

3 Institut d'Investigacions Biomèdiques August Pi i Sunyer (IDIBAPS), Barcelona, Spain

4 Catalan Institute of Nanoscience and Nanotechnology (ICN2), CSIC and The Barcelona Institute of Science and Technology (BIST), Campus UAB, Bellaterra, Barcelona, Spain

5 ICFO-Institut de Ciéncies Fotòniques, The Barcelona Institute of Science and Technology, Castelldefels, Barcelona, Spain

6 Institució Catalana de Recerca i Estudis Avançats (ICREA), Barcelona, Spain

*** Correspondence:**
anton.guimera@imb-cnm.csic.es; joseantonio.garrido@icn2.cat

Keywords: cortical spreading depression, DC-ECoG, graphene, infraslow.

Abstract

Recording infraslow brain signals (< 0.1 Hz) with microelectrodes is severely hampered by current microelectrode materials, primarily due to limitations resulting from voltage drift and high electrode impedance. Hence, most recording systems include high-pass filters that solve saturation issues but come in hand with loss of physiological and pathological information. In this work, we use flexible epicortical and intracortical arrays of graphene solution-gated field-effect transistors (gSGFETs) to map cortical spreading depression in rats and demonstrate that gSGFETs are able to record, with high-fidelity, infraslow signals together with signals in the typical local field potential bandwidth. The wide recording bandwidth results from the direct field-effect coupling of the active transistor, in contrast to standard passive electrodes, as well as from the electrochemical inertness of graphene. Taking advantage of such functionality, we envision broad applications of gSGFET technology for monitoring infraslow brain activity both in research and in the clinic.

Recently, there has been a particular resurgence of interest in fluctuations of brain activity occurring at < 0.1 Hz, commonly referred to as very slow, ultraslow or infraslow activity (ISA)[1]. ISA is suggested to have a unique neurophysiological basis[2], and to be indicative of brain states (e.g. sleep, anesthesia, coma, wakefulness)[2-4]. ISA is also correlated with resting-state networks in functional magnetic resonance imaging[5] and may significantly contribute to the high variability observed in the time course of physiological signals[6,7]. Interestingly, cortical spreading depression (CSD)[8,9], a slowly propagating wave of near-complete depolarization of neurons and astrocytes followed by a period of electrical activity suppression, occurs at infralow frequencies. CSD is often triggered in individuals suffering stroke or brain injury as well as migraines and recent research has shown that CSD plays a significant role in brain pathophysiology[10-12]. For this reason, monitoring electrophysiological signals below 0.1 Hz can be very valuable for clinical diagnosis, prognosis and therapy in neurocritical care[13-15].

Non-invasive techniques such as electroencephalography (EEG) and magnetoencephalography (MEG) have been used to study ISA[16,17]. However, their limited spatial resolution, and averaged signal impose serious limitations, e.g. scalp EEG alone is not sufficient for CSD detection[14,18]. Hence, invasive electrophysiological techniques are the most widely used to record infraslow brainwaves. The proper recording of ISA requires the use of direct-coupled amplifiers and extremely stable and low-impedance invasive electrodes. Traditionally, liquid-filled glass micropipettes are used, which allow only one or few-point measurements[19] and therefore impose serious mapping limitations. For higher spatial resolution and mapping, non-polarizable silver/silver chloride (Ag/AgCl) electrodes could be used, which prevent charge accumulation at the interface and therefore voltage drift. However, due to the toxicity of silver, the use of such electrodes for human or chronic animal *in vivo* monitoring is not an option[20]. This has fostered the search for alternative microelectrode materials with low impedance and drift, although none has yet been found capable of offering performance comparable to Ag/AgCl electrodes[21]. Current ISA recordings in humans are performed with platinum electrodes, which challenge CSD detection due to artefacts and transients[13]. Moreover, miniaturization of electrode size to achieve higher spatial resolution may cause intrinsic high-pass filtering of ISA due to the associated electrode impedance increase[22,23]. Other invasive optical techniques, such as calcium imaging are also used to monitor ISA, but still nowadays they present serious challenges in resolving high-frequency activity for a large number of neurons[24,25] and their intrinsic need of indicators limits the translation to clinical use. Consequently, there is a pressing need for a technique that allows measuring large-scale, high-spatiotemporal resolution electrophysiological signals including infralow frequencies in a potentially fully implantable, nontoxic, clinical-scale system. (Table S1).

As an alternative to the commonly used microelectrode technology, recording electrophysiological signals with field-effect transistors (FETs) offers several advantages: they are less sensitive to environmental noise thanks to their intrinsic voltage-to-current amplification, and they can be easily multiplexed[26]. Nonetheless, the difficulties in combining high gate capacitance and carrier mobility silicon FETs with flexible materials has historically hampered their use for *in vivo* recordings[27]. Graphene solution-gated field-effect transistors (gSGFETs) have been proposed to potentially overcome most previous drawbacks[28]. Graphene flexibility allows gSGFETs to be embedded in ultrasoft and flexible substrates without loss of performance[29], while its wide electrochemical window and biocompatibility allows direct contact with biological fluids and tissues and ensures a safe operation in *in vivo* conditions[30]. In addition, the two-dimensional nature of graphene provides the highest surface-to-volume ratio possible, making graphene very sensitive to charges at its surface. Taking advantage of the above-mentioned properties, in previous works, we demonstrated that gSGFETs are able to record local field potentials[31,32].

In this work, we investigate the potential of graphene microtransistors to record infraslow brain activity by performing *in vivo* recordings where we use, gSGFETs for both epicortical and intracortical mapping of cortical spreading depression. We found that graphene microtransistors are excellent devices for recording infraslow signals, performing similarly to solution-filled glass micropipettes while additionally offering the possibility of performing spatially-resolved mapping. Importantly, gSGFETs do not compromise the acquisition of signals in the conventional local field potential bandwidth, therefore allowing recording in a wide frequency bandwidth. Furthermore, we also demonstrate that gSGFET technology can be used in combination with optical techniques, such as laser speckle contrast imaging, to obtain 2-D maps of neurovascular coupling.

Fabrication and characterization of gSGFET arrays

A gSGFET is a device in which graphene is used as channel material, contacted by two metal leads (source and drain terminals), in direct contact with an electrolyte solution or conductive biological tissue where a reference electrode is placed and used as gate terminal (Fig. 1a). We fabricated 12 µm-thick flexible probes containing arrays of gSGFETs in both epicortical and intracortical designs (Fig. 1b) using the process previously reported[32]. The arrays were placed in zero insertion force connectors for interfacing with recording electronics (Fig. 1c). Characterization consisted in measuring the transfer curve, drain current (I_{ds}) vs gate-source voltage (V_{gs}), of all gSGFETs in each array with a fixed drain-source voltage (V_{ds}). The small dispersion of the charge neutrality point obtained (CNP=243.6 ± 6.1 mV), which is defined as the V_{gs} voltage associated to the minimum current value of the transfer curve, indicates the homogeneity of the transistors (Fig. 1d). Importantly, since V_{gs} and V_{ds} are shared, a small CNP dispersion allows near-optimal recording performance for all gSGFETs in the same array. The leakage current (I_{gs}) for all gSGFETs in the array was also measured, being in the nA range throughout the voltage sweep (Fig. 1e), demonstrating the good insulation of the passivation layer and the negligible reactivity of the graphene. Furthermore, we measured the frequency response of the transconductance (g_m), which indicates the efficiency of the signal coupling ($\partial I_{ds}/\partial V_{gs}$). The negative g_m for V_{gs} values lower than the CNP results in an inversion (180° phase) of the signals measured at such bias while for V_{gs} values higher than the CNP the signal phase is preserved. In both cases, we obtained constant g_m values in a wide bandwidth (Fig. 1f-g).

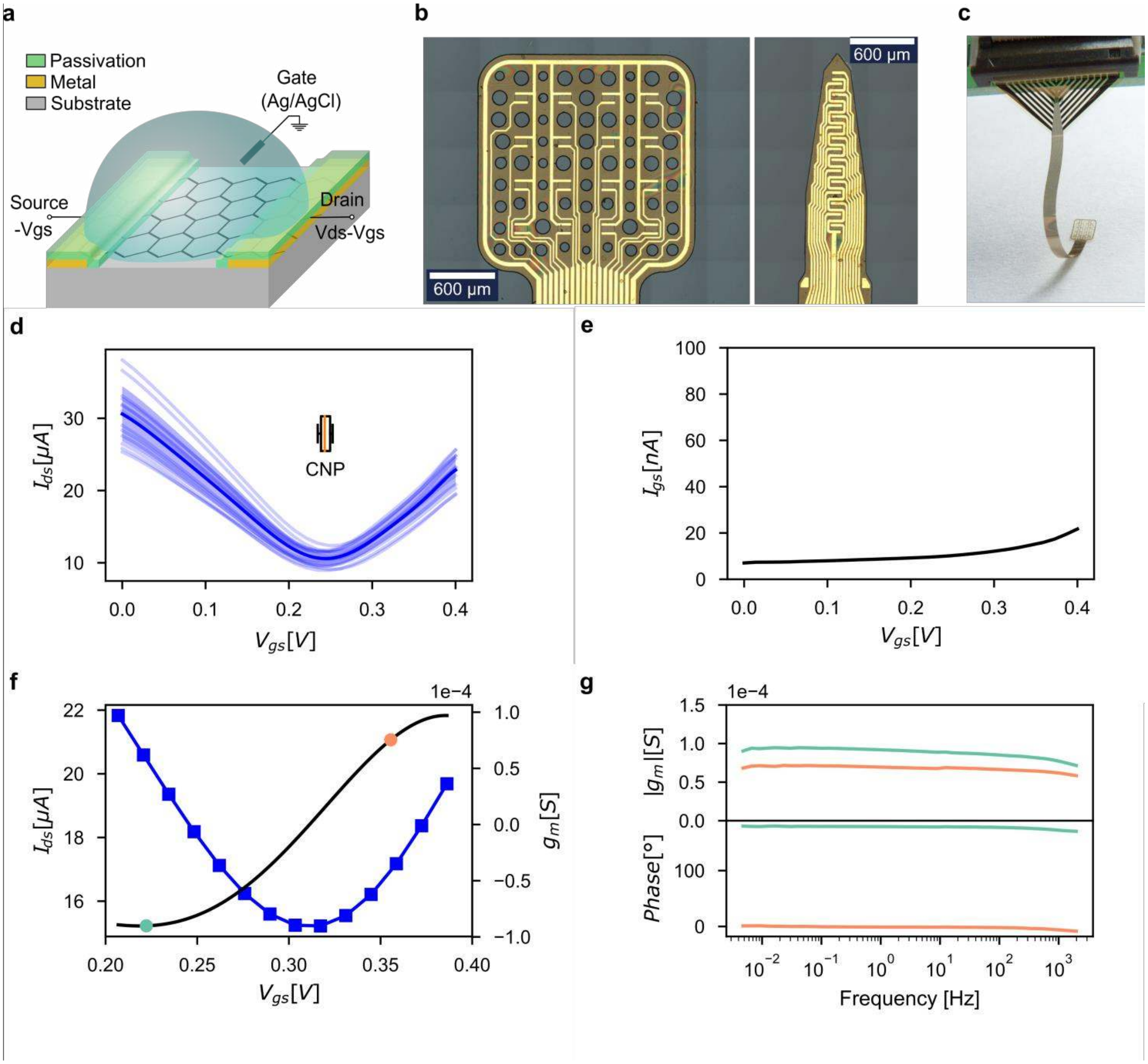

Fig. 1 | Flexible graphene solution-gated field-effect transistor array technology and characterization. a, Schematic of a graphene transistor polarized in common gate mode. **b**, Optical microscope images of the active area of a 4×4 gSGFET array and a 15 channel intracortical array. **c,** Photograph of the neural probe after peeling from the wafer and being introduced into a zero insertion force connector. **d-g,** Steady-state and frequency response characterization of a 100x50-µm^2 gSGFET array in 10 mM phosphate buffered saline (PBS) with a drain-source voltage bias (V_{ds}) of 50 mV. **d,** gSGFET transfer curves (blue lines), drain-source current (I_{ds}) *vs* gate-source voltage (V_{gs}), together with the mean (dark blue) and standard deviation (blue shade). Boxplot inset shows charge neutrality point dispersion (center line, median; box limits, upper and lower quartiles). **e,** Leakage current (I_{gs}) of all gSGFETs in the array throughout the voltage sweep. **f,** Transfer curve (blue squares and line) and its first derivative (transconductance (g_m), black line) of a gSGFET. **g,** Frequency response of the transconductance at two different points of the transfer curve (**f**): V_{gs} lower than the CNP (green), where g_m is negative resulting in a signal inversion (180º phase); and V_{gs} higher than the CNP (orange), where g_m is positive and thus results in no inversion (0º phase) . Independently of the branch of the transfer curve where a gSGFET is polarized, the module of g_m is similar to the steady-state value for a wide bandwidth (≈ 0 - 1 kHz).

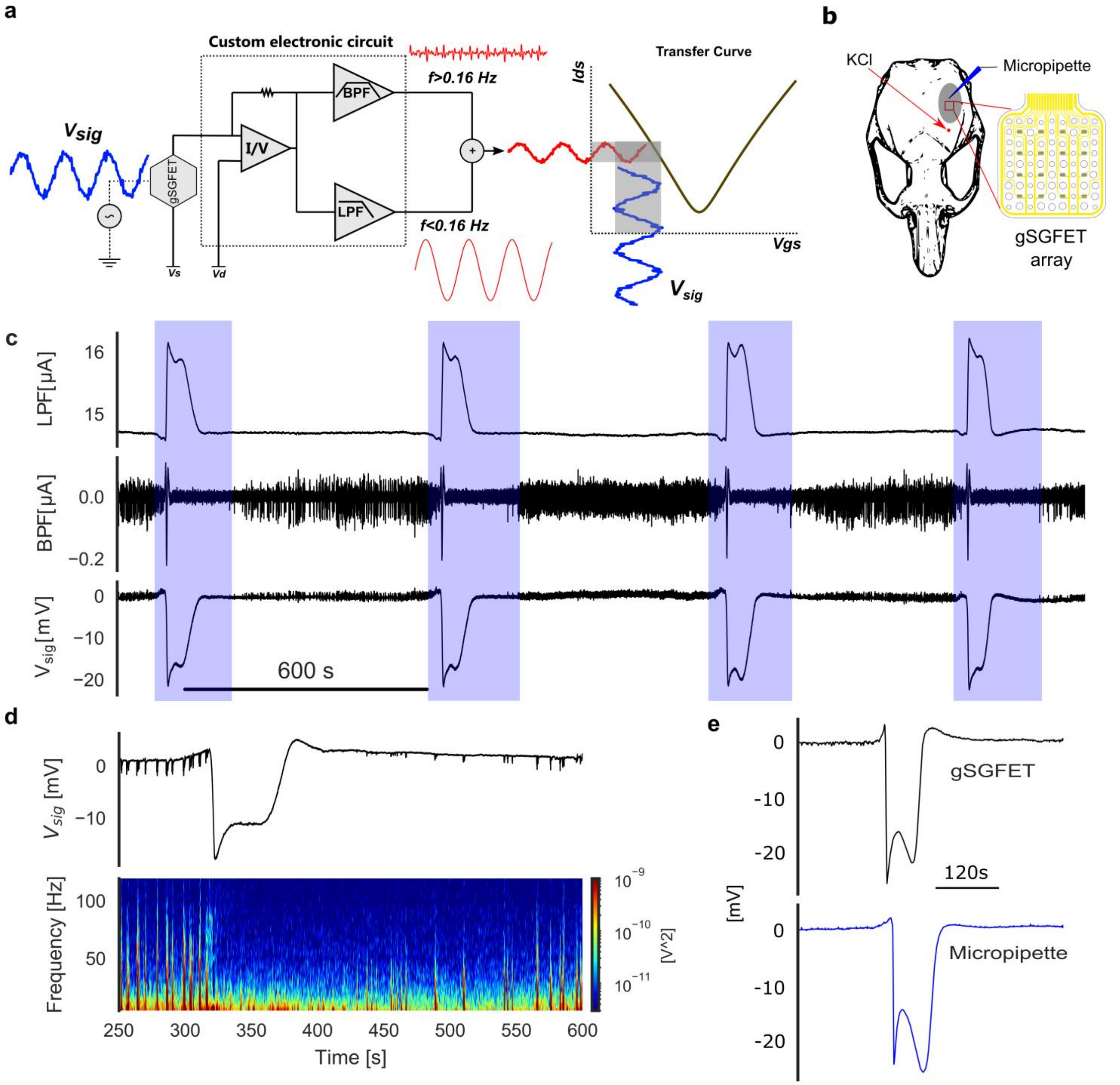

Fig. 2 | Infraslow, local field potential, and wide-band *in vivo* gSGFET recordings of cortical spreading depression (CSD). a, Schematic of the gSGFET recording setup and signal post processing methodology. The custom electronic circuit is used to perform the *in vivo* characterization (transfer curve) and record the transistor current in the low-pass-filtered (LPF) and the band-pass-filtered (BPF) bands. From the combination of both signals and taking into account the current-to-voltage conversion, the calibrated wide-band signal (V_{sig}) is obtained. **b,** Schematic of a rat skull depicting the craniotomy (grey area), the location of the gSGFET array and micropipette as also the frontal craniotomy where 5mM KCl was applied to induce CSDs. **c,** Electrophysiological recordings obtained with a gSGFET epicortical array during the induction of four CSD events (blue shade). From top to bottom: LPF signal, BPF and voltage-converted wide-band signal. **d,** Voltage-converted wide-band signal of a CSD event recorded by a gSGFET and spectrogram showing the characteristic silencing of activity. **e,** Comparison of a CSD signal recorded by a graphene transistor and a solution-filled glass micropipette with a Ag/AgCl wire demonstrating the excellent similarity in shape, magnitude and time span.

In vivo wide-band recordings with gSGFETs

Cortical spreading depression[10,12,19] was chosen to illustrate the capabilities of graphene transistors to record electrophysiological signals in a wide bandwidth. Experimentally, two craniotomies were performed over the left hemisphere of isoflurane-anaesthetized Wistar rats: a larger craniotomy over the primary somatosensory cortex, where the epicortical probe was placed, and a smaller one in the frontal cortex, where 5 mM KCl was applied locally to induce CSD (Fig. 2b). A custom electronic circuit allowed us to simultaneously record at two frequency bands: low-pass filtered band (LPF, ≈0-0.16 Hz) and band-pass filtered band (BPF, 0.16 Hz-10 kHz) with different gains (10^4, and 10^6 respectively) to avoid amplifier saturation due to the high-amplitude CSD signal. In a first set of experiments, we recorded the LPF and BPF signals with an epicortical gSGFET array during the induction of CSD events (Fig. 2c). The graphene transistors were polarized in the hole conduction regime, i.e. V_{gs} < CNP (negative g_m)resulting in an inversion of the recorded LPF and BPF current signals with respect to the voltage signal occurring at the gate. The LPF signal shows the very slow CSD event whereas the BPF signal corresponds to the local field potential, revealing the silencing of activity characteristic of cortical spreading depression. It is important to note that the high frequency content of the steep depolarization seen in the BPF signal at the beginning of each CSD event is generally the unique information of the CSD seen in AC-coupled recordings. After calibrationthe wide-band electrophysiological signal can be obtained (see Fig. 2 a, c and Data Analysis section in Methods). The calibration procedure eliminates both the variations associated with the different current levels and the transconductance differences at the bias point between the transistors (Fig. S1). In each CSD event a small positive shift of 1-2 mV generally precedes the depression, immediately after which a steep negative change (≈ -20 mV) can be observed, which slowly recovers during the next minute or so. The CSD-associated silencing of high-frequency activity and its progressive recovery is shown in the voltage wave and spectrogram of Fig. 2d. In order to confirm the fidelity of the CSD recordings of the gSGFET technology, simultaneous recordings with a solution-filled glass micropipette with a Ag/AgCl wire were conducted. The infraslow deflection associated with CSD as measured by gSGFETs has a very similar shape, magnitude and temporal duration than the signal recorded by a micropipette (see Fig.2e and Fig.S2: cross-correlation = 0.85 ± 0.1 for the recording of two CSD events).

ISA recording capabilities with gSGFETs and microelectrodes

A second set of experiments was designed to compare the performance of gSGFETs with microelectrodes in *in-vivo* direct-coupled recordings. CSD was induced and simultaneously recorded with an gSGFET epicortical array located more posterior to a neural probe containing groups of triodes of 50 µm diameter gold microelectrodes 200 µm apart in which one microelectrode of each triode was modified by deposition of platinum black to lower its impedance (Fig. S3). Data shown in Fig. 3 corresponds to a representative experiment of n=3 independent subjects. Fig. 3a shows that gold and platinum black recordings exhibit very large and diverse baseline offsets as well as oscillations and drifts (-7.9 ± 3.3 mV/h, n=10 and -3.6 ± 1.6 mV/h, n=6), while the gSGFET signals are very stable (1.1 ± 1.0 mV/h, n=15). Importantly, gSGFETs record significantly higher amplitudes for the CSD events (-13.3 ± 1.8 mV) in comparison with gold (-4.7 ± 1.6 mV) and platinum black (-

3.0 ± 0.7 mV) microelectrodes. Figure 3b highlights one of the intrinsic limitations of microelectrode technology for the measurement of ISA: polarization-induced drift.

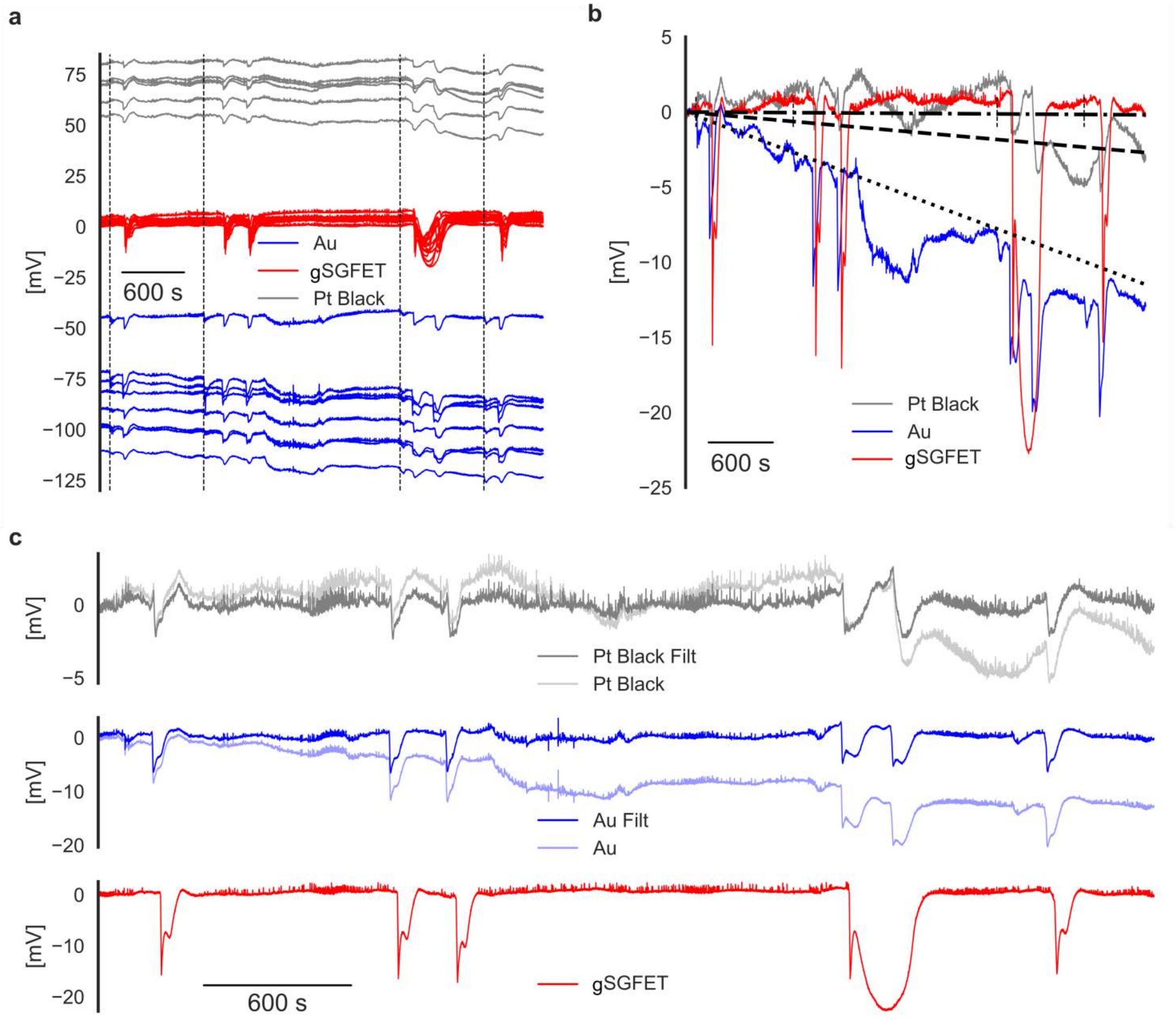

Fig. 3 | Comparison of DC-coupled gSGFET and microelectrode recordings of cortical spreading depression. a-c, Representative data of one of a total of three independent experiments. **a,** Direct-coupled recordings of 100 x 50 µm^2 gSGFET transistors and gold and platinum black 50 µm diameter microelectrodes. The vertical dashed lines show the time when KCl (5 mM) was applied to induce a CSD. **b,** DC-offset removed recordings of a representative channel of each type. Black lines illustrate the mean drift: dotted and dashed correspond to gold and platinum black microelectrodes, respectively, and the dash-dotted line corresponds to gSGFETs. **c,** DC-offset removed recordings of a representative channel of each type and the same signal filtered at 0.002 Hz to remove oscillations and drift; the gSGFET signal does not require any filtering and is therefore not distorted.

The drift of the baseline potential superimposed over the huge voltage offsets is problematic as it can lead to saturation of the amplifiers used to record the signal. More importantly, baseline oscillations in the infralow frequencies, will potentially hamper the determination of the exact characteristics of CSD, such as amplitude or waveform, as the required high-pass filter used to remove such effects will alter the signal shape (see Fig.3c and Fig. S4). Another intrinsic limitation of microelectrode technology is based on the relation between the microelectrode impedance and the input impedance of the recording equipment (Z_e' and Z_a', respectively)[21,23]. The recorded signal (V_{in}) is determined by the voltage divider formed by both impedances:

$$V_{in}(f) = I(f)Z_a'(f) \ = \frac{V_{sig}(f)\, Z_a'(f)}{Z_a'(f) + Z_e'(f)} \tag{1}$$

Eq. (1) implies that when Z_a' is not substantially larger than Z_e', the recorded signals will be attenuated and shifted with respect to V_{sig} [22]. It is important to highlight that the Z_a'>>Z_e' requirement to achieve a voltage gain equal to 1 could be compromised, especially at very-low frequencies, when the electrode area is scaled down, due to the inverse relation between electrode impedance and its area, leading to high-pass filtering of the recorded signals. By measuring the impedance of both electrode types and modelling the preamplifier impedance with the values reported by the manufacturer, we obtained the voltage gain (V_{in}/V_{sig}) of the equivalent circuit formed by the recording electrode and the amplifier, see Fig. 4a-b.Fig. 4c shows a representative CSD recorded by a gSGFET and gold and platinum black microelectrodes and the mean amplitude of the first peak for each type. For the 50 µm diameter gold microelectrodes, an attenuation lower than 50% is expected from Fig. 4b, which is in agreement with the experimental results. For the platinum black electrodes we tentatively attribute the higher than predicted attenuation to *in vivo* electrochemical processes that impact the electrode response at very low frequencies[33]. We assign the superior performance of gSGFETs to the following main reasons. First, graphene exhibits an excellent DC stability, as demonstrated by low *in vivo* drift. We attribute this to the low density of states of pristine graphene near the Fermi level, which decreases the overall electronic overlap with redox species[34], and to the low density of extrinsic electron transfer sites, i.e. defects and edges, all contributing to the excellent electrochemical inertness of CVD graphene[24,35,36]. The low leakage current measured (Fig. 1e) also supports the electrochemical inertness.

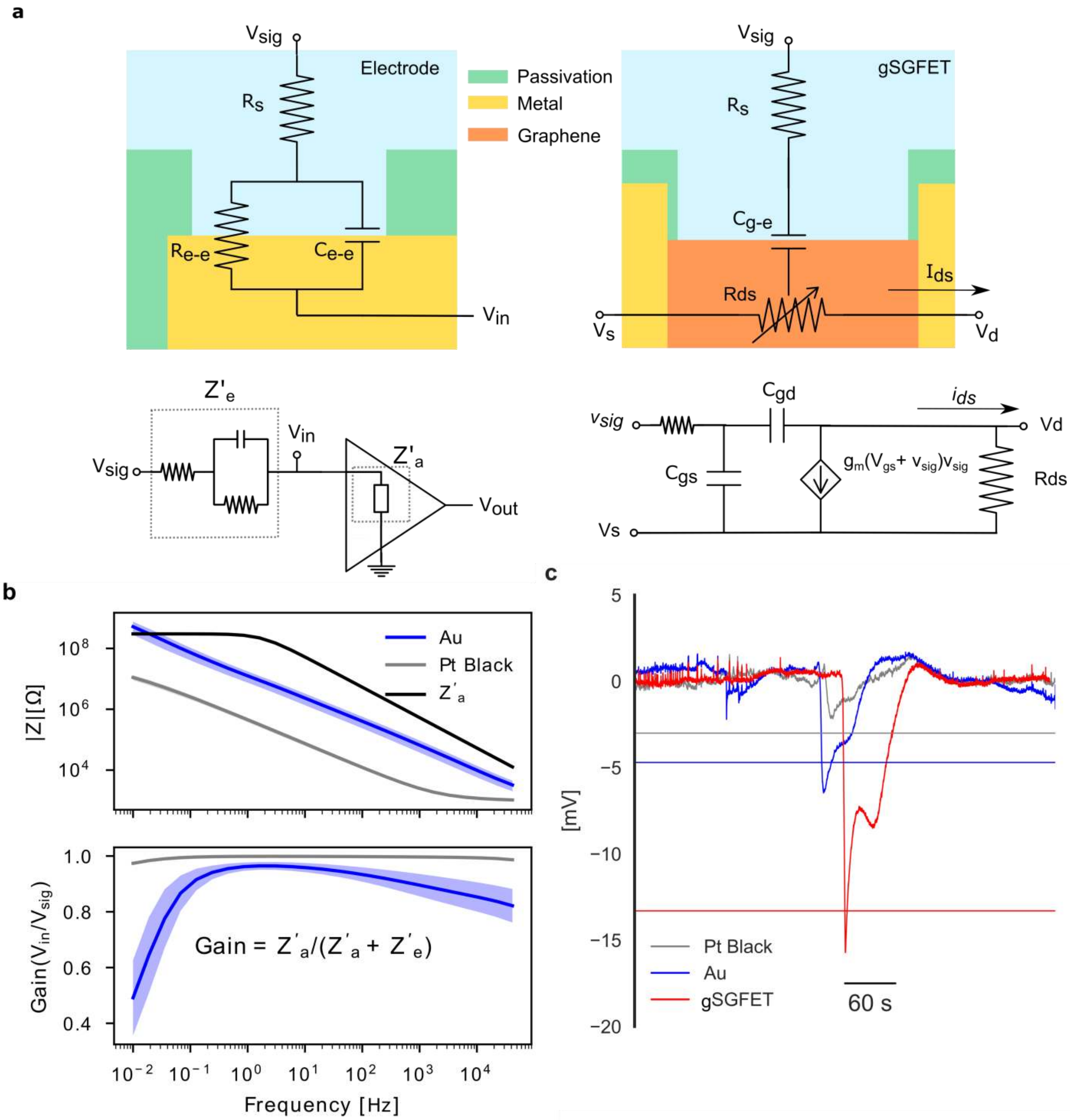

Fig. 4 | Microelectrode and gSGFET recording modes: considerations for infraslow recordings. a, Cross-sectional view and superimposed electric equivalent circuit models of a recording electrode and a gSGFET. For an electrode, the electrode-electrolyte interface, is modelled simply as a capacitor and a resistor in parallel ($R_{e\text{-}e}$, $C_{e\text{-}e}$). V_{in}, the voltage at the input of the amplifier is determined by the voltage divider formed by Z'_e and Z'_a, the effective electrode and amplifier impedance, respectively. R_s represents the electrolyte resistance. In the case of a gSGFET, V_{sig} modulates the graphene channel resistance (R_{ds}) by field-effect through the gate capacitance ($C_{g\text{-}e}$), which results in current variations (i_{ds}) proportional to the transconductance value at the bias point, plus the voltage signal (which is mostly negligible for small amplitude electrophysiological signals), as seen in the small signal model. **b,** Mean and standard deviation of the impedance module (experimental data) of nine 50 µm diameter gold (blue) and six platinum black (grey) microelectrodes together with Z'_a and calculated voltage gain (V_{in}/V_{sig}) for each microelectrode type. **c,** Recordings of a CSD event for each type of microelectrodes and a gSGFET. Horizontal lines represent the mean value of CSD amplitude.

The second reason why graphene microtransistors can record infraslow signals is related to their working mechanism, which is significantly different from that of electrodes. In gSGFETs, voltage oscillations near the active graphene channel modulate the current flow along it (see schematic and small-signal model in Fig. 4a). Eq. 2 shows the relation between the recorded current ($\mathrm{I_{ds-rec}}$) and the signal ($\mathrm{V_{sig}}$):

$$I_{ds-rec}\left(V_{gs},V_{sig}\right)=I_{ds}\left(V_{gs}\right)\;+\;i_{ds}\left(V_{gs},V_{sig}\right)=I_{ds}\left(V_{gs}\right)\;+g_{m}\left(V_{gs}+V_{sig}\right)V_{sig},\qquad(2)$$

where $\mathrm{I_{ds}}$ is the current at the bias point $\mathrm{V_{gs}}$ and $\mathrm{i_{ds}}$ the current variation induced by the gate signal. This equation is valid and frequency-independent as long as g_m is also frequency-independent. In this work (Fig. 1g), we provide evidence that the transconductance of gSGFETs remains constant in a wide bandwidthand and that this behaviour is preserved with further downscaling of gSGFETs (Fig.S5).

Mapping cortical spreading depression with gSGFETs

As an example of the potential of gSGFET technology, we mapped the propagation of CSD events using a 4x4 epicortical gSGFET array and compared the signals with what is observed in conventional high-pass filtered recordings (Fig. 5a-b). The recording of the CSD event with the gSGFET array reveals that while the onset of the negative shift is similar for all gSGFETs, there is much more variety in the subsequent recovery, with some transistors exhibiting a second negative shift with higher amplitude than the first one. This effect can also be observed in the last two frames (corresponding to 80 s and 90 s) of the spatial maps of gSGFET recordings (Fig. 5b) where recovered and still depressed brain areas coexist. Importantly, this information is lost in conventional microelectrode recordings, where only the CSD onset is observed due to the high pass filter in the recording electronics. We found that the mean duration of CSD events is 47 ± 8 s and a speed of propagation of 8 ± 1 mm/min (n=10 CSDs collected from two different subjects).

Under physiological conditions, there is a neurovascular response, vasodilatation and increased regional cerebral blood flow (rCBF) due to spreading depolarization that causes spreading hyperemia[10]. However, most studies on CSD neurovascular coupling have been performed with mapping techniques for the rCBF while electrical activity is measured only at two sites with glass micropippetes[5]. Here, taking advantage of the gSGFET technology, we designed an experiment in which we could simultaneously map both variables. Fig. 5c provides further evidence of the spreading depolarization and hyperemia neurovascular coupling. We used a non-contact, wide-field technique, laser speckle contrast imaging (LSCI)[37], that allows imaging variations of rCBF[38]. Experimentally, a craniotomy was performed in a Wistar rat and a continuous-wave temperature controlled laser diode and a camera were mounted to image a wide area inside in which an epicortical 16-channel gSGFET array was placed. After 5mM KCl administration, CSD was induced, which was followed by an increase in rCBF that slowly returned (4-5minutes) to basal values (Fig. 5c).

We also performed *in vivo* experiments with intracortical probes consisting of a linear array of 15 gSGFETs spanning the entire depth of a rat cortex (Fig. 6a). From both the ordered recording and the spatiotemporal voltage map (Fig. 6b), it can be seen how CSD occurs in the whole cortex depth. A transition from a superficial long depolarization to a shorter one preceded and followed by a hyperpolarization in the deeper layers can be clearly observed.

Outlook

In this work we show that gSGFETs can record neural signals in a wide electrophysiological bandwidth, from infralow (<0.1 Hz) frequencies to the typical local field potential bandwidth, similar to solution-filled glass micropipettes but with the capability of overcoming their spatial sampling limitations. Importantly, this capability does not depend on a given transistor size but is preserved among a wide range of device sizes, which brings freedom when designing an array for a given application. There are two main reasons that explain this unique recording capability: the direct DC-coupling of transistors, in contrast to standard passive electrodes; and the excellent electrochemical stability of graphene. Making use of these features, gSGFET technology opens the possibility of mapping infraslow oscillations with high fidelity and spatial resolution (epicortically and intracortically). This can lead to a better understanding of the brain regions where ISA is initiated, its propagation to other areas and a clarification of the interplay of different cellular types, which are still poorly understood[1,2,39]. Additionally, the wide recording bandwidth of gSGFETs can help in determining the relation between ISA and higher frequency signals[17,40] and contribute to a better understanding of the genesis of local field potentials[41] and of cortical wave propagation features[42,43].

Since 2014, work exploiting both the transparency and electrical conductivity of graphene has allowed simultaneous local field potential recordings using graphene microelectrodes, and imaging or optical stimulation at the same position, which has profound implications in neuroscience[24,44]. Our work demonstrates that graphene transistors can be used together with imaging techniques, such as LSCI to map infraslow electrophysiological signals and regional cerebral blood flow. This combination of techniques holds great potential and can contribute to a better understanding of neurovascular coupling phenomena.

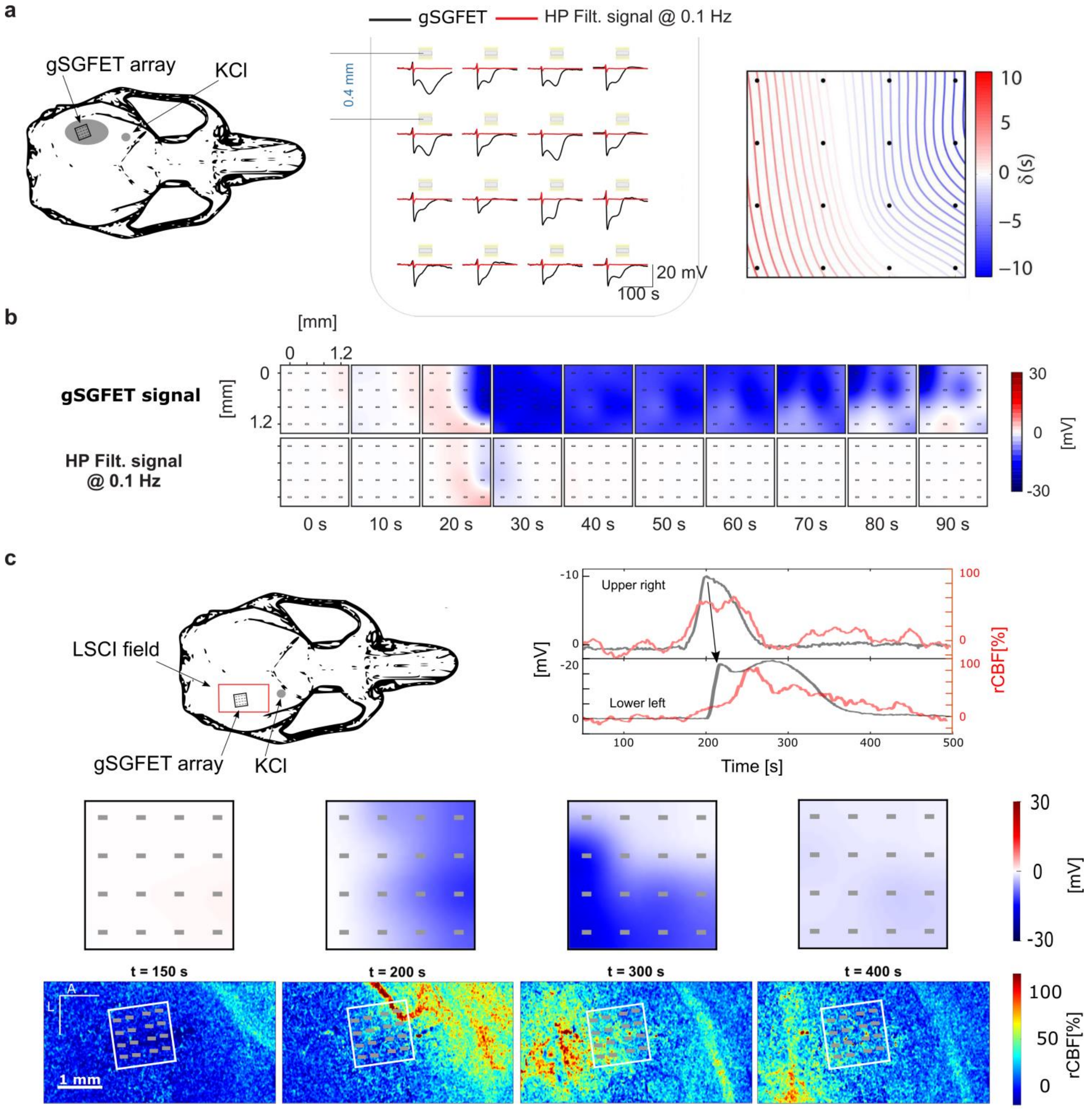

Fig. 5 | Mapping cortical spreading depression with graphene transistors. a, Infralow frequency signals recorded by a 4x4, 400 µm grid spacing, gSGFET array (black lines) during the occurrence of a CSD event as illustrated in the top left schematic. The contour plot shows the time delays of the onset of CSD with respect to the mean time illustrating the spatiotemporal course of the CSD. **b,** Interpolated spatial voltage maps showing the propagation of the same CSD event as measured by the gSGFET array. **a,b** High pass filtered recordings at 0.1Hz (red lines in **a** and bottom spatial voltage maps in **b**) are included to illustrate the loss of signal information in conventional microelectrode recordings. **c,** Schematic of a rat skull depicting the laser speckle contrast imaging field-of-view and the position of the gSGFET array. Electrical recordings and optical imaging were performed directly on the cortical surface. Time evolution of the upper right and lower left graphene microtransistors as well as the regional cerebral blood flow (rCBF) measured at the same position showing their co-occurrence. Colour maps represent the spatial value of the extracellular voltage as measured by the gSGFET array (top) and the rCBF (bottom) at a given set of times after the induction of a CSD event. Representative data of one of a total of two independent experiments.

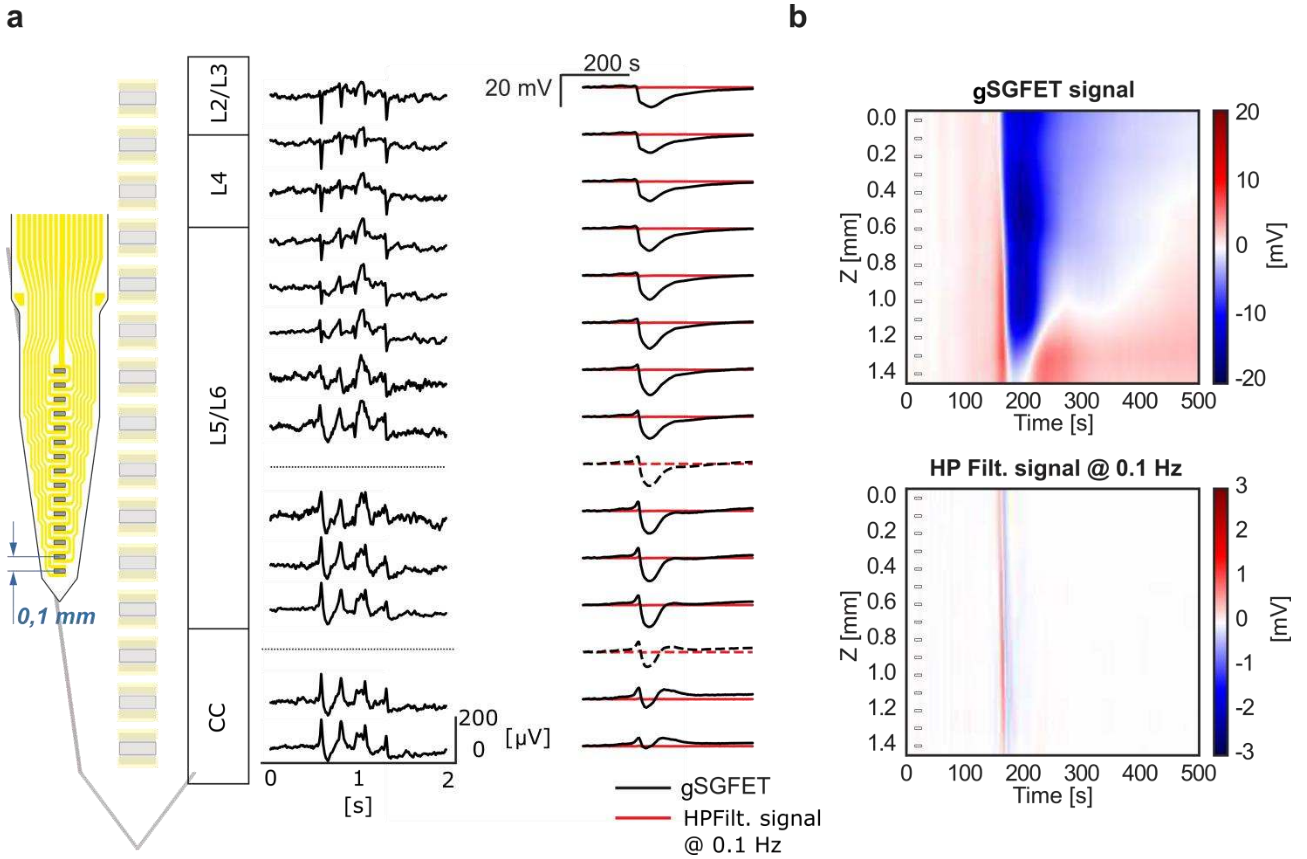

Fig. 6 | Depth profile of the infralow-frequency voltage variations induced by cortical spreading depression in a rat cortex. a, Layout of the fabricated 15-channel graphene intracortical probe and ordered local field potential recordings. Infralow-frequency recordings (black lines) during the occurrence of a CSD event. Dashed lines, have been interpolated from nearby transistors. Depth position is indicated by the layer number and corpus callosum (CC). **b,** Colour maps of the temporal course of the infraslow changes during a CSD event across the depth of a rat cortex. **a-b,** Same signal high-pass filtered at 0.1 Hz (red lines) and their spatio-temporal colour map are included to illustrate the loss of information in conventional microelectrode recordings.

In the particular case of CSD, where no non-invasive electrophysiological technique has been demonstrated capable of its monitoring, the adoption of invasive DC-coupled electrode recordings has been proposed to provide further diagnostic information and easy and direct detection of CSDs[13]. gSGFET technology emerges as a potential preclinical as well as clinically relevant tool to help determine the relation of CSDs to neural disorders such as migraine, malignant stroke, subarachnoid and intracranial haemorrhage, and traumatic brain injury. If the challenges of translating gSGFET technology to the clinics, such as chronic and safe operation and human compatibility are surpassed, gSGFETs could be applied in neurointensive care monitoring[12,14]or for CSD intraoperative monitoring since there is evidence that CSD can occur during neurosurgical procedures[45]. Importantly,in contrast to electrodes where a signal is needed to measure electrode impedance, the possibility to measure the characteristic transfer curve of a gSGFET *in vivo* at any time, allows assessing the stability as well as the signal coupling magnitude (transconductance) during an implant lifetime, therefore easing the evaluation of its chronic performance. In summary, our work demonstrates that gSGFET arrays are ideal candidates to fill the gap of a large-scale, high-spatiotemporal recording technology that covers a wide electrophysiological bandwidth in a potentially fully implantable, nontoxic, clinical-scale device. By measuring the full bandwidth of brain activity with high spatiotemporal resolution we will be able to improve our understanding of brain function in health and disease status, and develop better diagnostic and therapeutic procedures for those affected.

References

1 Hughes, S. W., Lőrincz, M. L., Parri, H. R. & Crunelli, V. in *Progress in Brain Research* Vol. 193 (eds Eus J. W. Van Someren *et al.*) 145-162 (Elsevier, 2011).

2 Mitra, A. *et al.* Spontaneous Infra-slow Brain Activity Has Unique Spatiotemporal Dynamics and Laminar Structure. *Neuron*, doi:https://doi.org/10.1016/j.neuron.2018.03.015.

3 Lecci, S. *et al.* Coordinated infraslow neural and cardiac oscillations mark fragility and offline periods in mammalian sleep. *Science Advances* **3**, e1602026 (2017).

4 Mitra, A., Snyder, A. Z., Tagliazucchi, E., Laufs, H. & Raichle, M. E. Propagated infra-slow intrinsic brain activity reorganizes across wake and slow wave sleep. *Elife* **4** (2015).

5 Hiltunen, T. *et al.* Infra-slow EEG fluctuations are correlated with resting-state network dynamics in fMRI. *Journal of Neuroscience* **34**, 356-362 (2014).

6 Leopold, D. A., Murayama, Y. & Logothetis, N. K. Very slow activity fluctuations in monkey visual cortex: implications for functional brain imaging. *Cerebral cortex* **13**, 422-433 (2003).

7 Kelly, A. C., Uddin, L. Q., Biswal, B. B., Castellanos, F. X. & Milham, M. P. Competition between functional brain networks mediates behavioral variability. *Neuroimage* **39**, 527-537 (2008).

8 Chung, D. Y. & Ayata, C. in *Primer on Cerebrovascular Diseases (Second Edition)* (eds José Biller *et al.*) 149-153 (Academic Press, 2017).

9 Hartings, J. A. *et al.* The continuum of spreading depolarizations in acute cortical lesion development: examining Leão's legacy. *Journal of Cerebral Blood Flow & Metabolism* **37**, 1571-1594 (2017).

10 Dreier, J. P. The role of spreading depression, spreading depolarization and spreading ischemia in neurological disease. *Nat Med* **17**, 439-447 (2011).

11 Dreier, Jens P. & Reiffurth, C. The Stroke-Migraine Depolarization Continuum. *Neuron* **86**, 902-922, doi:https://doi.org/10.1016/j.neuron.2015.04.004 (2015).

12 Lauritzen, M. *et al.* Clinical relevance of cortical spreading depression in neurological disorders: migraine, malignant stroke, subarachnoid and intracranial hemorrhage, and traumatic brain injury. *Journal of Cerebral Blood Flow & Metabolism* **31**, 17-35 (2011).

13 Hartings, J. A. *et al.* Direct current electrocorticography for clinical neuromonitoring of spreading depolarizations. *Journal of Cerebral Blood Flow & Metabolism* **37**, 1857-1870 (2017).

14 Dreier, J. P. *et al.* Recording, analysis, and interpretation of spreading depolarizations in neurointensive care: review and recommendations of the COSBID research group. *Journal of Cerebral Blood Flow & Metabolism*, 0271678X16654496 (2016).

15 Kovac, S., Speckmann, E.-J. & Gorji, A. Uncensored EEG: The role of DC potentials in neurobiology of the brain. *Progress in Neurobiology*, doi:https://doi.org/10.1016/j.pneurobio.2018.02.001 (2018).

16 Vanhatalo, S., Voipio, J. & Kaila, K. Full-band EEG (FbEEG): an emerging standard in electroencephalography. *Clinical Neurophysiology* **116**, 1-8, doi:http://dx.doi.org/10.1016/j.clinph.2004.09.015 (2005).

17 Vanhatalo, S. *et al.* Infraslow oscillations modulate excitability and interictal epileptic activity in the human cortex during sleep. *Proceedings of the National Academy of Sciences of the United States of America* **101**, 5053-5057 (2004).

18 Hofmeijer, J. *et al.* Detecting Cortical Spreading Depolarization with Full Band Scalp Electroencephalography: An Illusion? *Frontiers in Neurology* **9**, doi:10.3389/fneur.2018.00017 (2018).

19 Ayata, C. & Lauritzen, M. Spreading depression, spreading depolarizations, and the cerebral vasculature. *Physiological reviews* **95**, 953-993 (2015).

20 Stensaas, S. S. & Stensaas, L. J. Histopathological evaluation of materials implanted in the cerebral cortex. *Acta Neuropathologica* **41**, 145-155, doi:10.1007/bf00689766 (1978).

21 Li, C. *et al.* Evaluation of microelectrode materials for direct-current electrocorticography. *Journal of neural engineering* **13**, 016008 (2015).

22 Nelson, M. J., Pouget, P., Nilsen, E. A., Patten, C. D. & Schall, J. D. Review of signal distortion through metal microelectrode recording circuits and filters. *Journal of neuroscience methods* **169**, 141-157 (2008).

23 Stacey, W. C. *et al.* Potential for unreliable interpretation of EEG recorded with microelectrodes. *Epilepsia* **54**, 1391-1401 (2013).

24 Kuzum, D. *et al.* Transparent and flexible low noise graphene electrodes for simultaneous electrophysiology and neuroimaging. *Nature communications* **5**, 5259 (2014).

25 Deneux, T. *et al.* Accurate spike estimation from noisy calcium signals for ultrafast three-dimensional imaging of large neuronal populations in vivo. *Nature Communications* **7**, 12190, doi:10.1038/ncomms12190

https://www.nature.com/articles/ncomms12190#supplementary-information (2016).

26 Fang, H. *et al.* Capacitively coupled arrays of multiplexed flexible silicon transistors for long-term cardiac electrophysiology. *Nature biomedical engineering* **1**, 0038 (2017).

27 Heremans, P. *et al.* Mechanical and electronic properties of thin-film transistors on plastic, and their integration in flexible electronic applications. *Advanced Materials* **28**, 4266-4282 (2016).

28 Hess, L. H., Seifert, M. & Garrido, J. A. Graphene transistors for bioelectronics. *Proceedings of the IEEE* **101**, 1780-1792 (2013).

29 Kim, B. J. *et al.* High-Performance Flexible Graphene Field Effect Transistors with Ion Gel Gate Dielectrics. *Nano Letters* **10**, 3464-3466, doi:10.1021/nl101559n (2010).

30 Kostarelos, K., Vincent, M., Hebert, C. & Garrido, J. A. Graphene in the Design and Engineering of Next-Generation Neural Interfaces. *Advanced Materials* **29** (2017).

31 Benno, M. B. *et al.* Mapping brain activity with flexible graphene micro-transistors. *2D Materials* **4**, 025040 (2017).

32 Hébert, C. *et al.* Flexible Graphene Solution-Gated Field-Effect Transistors: Efficient Transducers for Micro-Electrocorticography. *Advanced Functional Materials* **28**, 1703976, doi:doi:10.1002/adfm.201703976 (2018).

33 Shinwari, M. W. *et al.* Microfabricated Reference Electrodes and their Biosensing Applications. *Sensors* **10**, 1679 (2010).

34 Chen, S., Liu, Y. & Chen, J. Heterogeneous electron transfer at nanoscopic electrodes: importance of electronic structures and electric double layers. *Chemical Society Reviews* **43**, 5372-5386 (2014).

35 Brownson, D. A. & Banks, C. E. The electrochemistry of CVD graphene: progress and prospects. *Physical Chemistry Chemical Physics* **14**, 8264-8281 (2012).

36 Brownson, D. A. C., Munro, L. J., Kampouris, D. K. & Banks, C. E. Electrochemistry of graphene: not such a beneficial electrode material? *RSC Advances* **1**, 978, doi:10.1039/c1ra00393c (2011).

37 Valdes, C. P. *et al.* Speckle contrast optical spectroscopy, a non-invasive, diffuse optical method for measuring microvascular blood flow in tissue. *Biomedical optics express* **5**, 2769-2784 (2014).

38 Boas, D. A. & Dunn, A. K. Laser speckle contrast imaging in biomedical optics. *Journal of biomedical optics* **15**, 011109 (2010).

39 Shibata, M. & Suzuki, N. Exploring the role of microglia in cortical spreading depression in neurological disease. *Journal of Cerebral Blood Flow & Metabolism* **37**, 1182-1191, doi:10.1177/0271678x17690537 (2017).

40 Mitra, A. & Raichle, M. E. How networks communicate: propagation patterns in spontaneous brain activity. *Phil. Trans. R. Soc. B* **371**, 20150546 (2016).

41 Herreras, O. Local field potentials: myths and misunderstandings. *Frontiers in neural circuits* **10**, 101 (2016).

42 Massimini, M., Huber, R., Ferrarelli, F., Hill, S. & Tononi, G. The sleep slow oscillation as a traveling wave. *Journal of Neuroscience* **24**, 6862-6870 (2004).

43 Capone, C. *et al.* Slow Waves in Cortical Slices: How Spontaneous Activity is Shaped by Laminar Structure. *Cerebral Cortex*, 1-17 (2017).

44 Park, D.-W. *et al.* Graphene-based carbon-layered electrode array technology for neural imaging and optogenetic applications. *Nature communications* **5**, ncomms6258 (2014).

45 Carlson, A. P. *et al.* Cortical spreading depression occurs during elective neurosurgical procedures. *Journal of neurosurgery* **126**, 266-273 (2017).

Acknowledgments

This work was funded by the European Union's Horizon 2020 research and innovation programme under Grant Agreement No. 696656 (Graphene Flagship) and No. 732032 (BrainCom). This work has made use of the Spanish ICTS Network MICRONANOFABS partially supported by MINECO and the ICTS 'NANBIOSIS', more specifically by the Micro-NanoTechnology Unit of the CIBER in Bioengineering, Biomaterials & Nanomedicne (CIBER-BBN) at the IMB-CNM. E.M.C. worked in this manuscript during the PhD in Electrical and Telecommunication Engineering at the Universitat Autònoma de Barcelona. E. d. C. thanks to Spanish Ministerio de Economía y Competitividad for the Juan de la Cierva postdoctoral grant IJCI-2015-25201. T. Du acknowledges support from Fundació CELLEX Barcelona, Ministerio de Economía y Competitividad /FEDER (PHOTODEMENTIA, DPI2015-64358-C2-1-R), the "Severo Ochoa" Programme for Centres of Excellence in R&D (SEV-2015-0522) and the Obra social "la Caixa" Foundation (LlumMedBcn).

Author contributions

E.M.C. did most of the fabrication and characterization of the gSGFET arrays, contributed to the design and performance of the *in vivo* experiments, analyzed the data and wrote the manuscript. X.I. designed the neural probes and fabricated the microelectrode arrays. A.B.C. contributed to the fabrication and characterization of the gSGFET arrays. M.D. performed the *in vivo* experiments. P.G., C.H., J.B. and E.P.A. contributed to the growth of the CVD graphene. E.P.A., E.dC. and J.M.dC.S. contributed to the transfer of graphene. E.P.A., E.dC.G. and G.R. contributed to the characterization of CVD graphene. J.M.A. contributed to the fabrication of the custom electronic instrumentation and development of a python-based user interface. A.C. contributed to the CSD propagation analysis. R.G.C. contributed in the noise characterization and analysis of the devices. T.Dr., E.V. and T.Du. contributed to the *in vivo* measurements and analysis of cerebral blood flow. M.D., M.S.V., A.G.B, R.V. and J.A.G. participated in the design of the *in vivo* experiments and thoroughly reviewed the manuscript. A.G.B. contributed in the design and fabrication of the custom electronic instrumentation, development of a custom gSGFET python library and in the analysis of the data. All authors read and reviewed the manuscript.

Competing interests

Patent application (nº P201831068) filled by CSIC, ICREA, CIBER, ICN2 and IDIBAPS; inventors: A.G.B., E.M.C., X.I., R.V., M.S.V. and J.A.G.; concerning a graphene transistor system for measuring electrophysiological signals (pending).

Methods

Graphene growth and characterization

Graphene layers were grown by Chemical Vapor Deposition (CVD) using one of the following procedures: a) A lamp-heated rapid thermal CVD equipment from Jipelec and 25 μm thick, 99.8 % metal basis copper foil provided by AlfaAesar have been employed. Prior to graphene CVD growth, copper foils were sequentially cleaned in acetic acid and acetone, and finally rinsed in isopropyl alcohol (IPA). Sample dimensions were 6 x 5 cm^2. Growth processing conditions consisted in 10 minutes at 750 °C, 200 sccm H_2 plus 5 minutes at 800 °C, 25 sccm CH_4 / 200 sccm H_2. b) Chemical vapour deposition was on a 4.5x7 cm^2 copper foil (Alfa Aesar, annealed, Coated). Prior to the growth, the copper foil was electropolished during 5 min at a fixed current density of 62 mA/cm^{-2} in a solution containing H_20 (1 L) + H_3PO_4 (0.5 L) + ethanol (0.5 L) + isopropanol (0.1 L) and urea (10 g). Then, the copper foil was loaded in a planar quartz tube (1600x60 mm) and heated by a three zone oven. A first annealing step at 1015 ºC under a 400 sccm argon flow at 100 mbar during 1 h was followed by a 15-min growth step at 12 mbar under a gas mixture of 1000 sccm argon, 200 sccm hydrogen and 2 sccm of methane. The sample was then cooled down under a 400 sccm argon flow by removing the quartz tube from the oven. For all samples, a complete Raman characterization was performed using a Witec spectrograph (Fig.S6a-d). Raman maps of 30x30 μm^2 were registered with a spatial resolution lower than 1 μm^2 (using a 50x objective). We used a 488 nm excitation wavelength to minimize the copper substrate luminescence signal. The laser power was kept below 1.5 mW to avoid sample heating and a 600 g/nm grating was used to provide a pixel to pixel spectral resolution below 3 cm^{-1}.

gSGFET array fabrication and characterization

Four-inch silicon wafers were used as a support to build the devices. First, a 10-µm-thick polyimide layer (PI-2611, HD MicroSystems) was spin-coated to be used as substrate and hard-baked at 350ºC to complete the imidation process. Graphene transistors were fabricated in a sandwich-like structure. For that, a first layer of metal (Ti/Au, 10/100 nm) was evaporated and defined in a standard lift-off process using the image reversal photoresist AZ5214E (Clariant GmbH, Germany). Then, single-layer graphene was transferred by electrochemical delamination[46]. After removing the PMMA protection layer, the graphene active areas were defined by means of an oxygen-based reactive ion etching (RIE). A second metal layer (Ni/Au, 20/200nm) was evaporated and defined in a similar standard lift-off process avoiding the use of ultrasounds in order to maintain graphene integrity. SU-8 (SU-8 2005, MicroChemCorp., USA) a permanent epoxy-based negative photoresist was used to passivate the metal leads while defining the graphene channel and metal contacts. Finally, the polyimide substrate was structured in a deep-RIE process using the thick AZ9260 positive photoresist (Clariant GmbH, Germany) as an etching mask. Polyimide probes were directly peeled off from the wafer and placed in a zero insertion force (ZIF) connector to be interfaced with our custom electronic instrumentation. Current-voltage measurements of graphene transistors were performed in common gate mode with a fixed drain-source voltage (V_{ds}=50 mV) varying the gate-source voltage (V_{gs}) vs. a Ag/AgCl reference electrode in 0.01 M PBS solution. Steady-state was ensured by acquiring only after time derivative of 1 s of current is below 5e-7 A/s. The total leakage current was measured for the whole array and corresponds to the sum of the individual leakage currents of all transistors in the array. The frequency response of the transconductance was measured by applying a sum of sinusoidal signals at the electrolyte solution through the reference electrode and by measuring the modulation of the drain current. The acquired signals were splitted into two bands, low frequencies (≈0-10 Hz) in which drain-source current was simultaneous acquired for all transistors in an array, and higher frequencies (10 Hz-30 kHz) in which each transistor was recorded individually (Fig. S7). Data reporting the root-mean-square gate voltage noise dependence on transistor area is included in Supplementary Figure S8 for a better characterization of current gSGFET technology.

Microelectrode array fabrication and characterization

The flexible microelectrode array was fabricated in polyimide in a very similar process. Here, a Ti/Au (20/200 nm) metal layer was evaporated on a 10 µm-thick polyimide-covered four-inch silicon wafer to define the metal tracks and the microelectrodes, while a second polyimide layer (2 µm thick) was used as the passivation layer. Two subsequent etching steps were used to open, firstly, the microelectrode active areas and, secondly, to structure the polyimide in order to define the probe geometry which is the same as in Illa et. al.[47]. Platinum black was deposited in some electrodes (Fig. S3a) by constant polarization amperometry. A voltage of -0.2V against a Ag/AgCl reference electrode was applied during 15 s. Impedance spectra were measured against a Ag/AgCl reference electrode using a Solartron SI 1260 equipment (Solarton analytical, UK) with 20 mV signal amplitude (Fig. S3b).

Ethical approval and animal handling

All experimental procedures were conducted in accordance with the European Union guidelines on protection of vertebrates used for experimentation (Directive 2010/63/EU of the European Parliament and of the Council of 22 September 2010) and all experiments were approved by the ethics committee of the Hospital Clinic de Barcelona. Rats were kept under standard conditions (room temperature 23 ±1ºC, 12:12-h light-dark cycle, lights on at 08:00), with food (A04, Harlan, Spain) and water available ad libitum.

In vivo recordings

Eleven adult male Wistar rats (225-375 g) were used in this study. Animals were deeply anaesthetized with isoflurane (4% induction, 1-3% maintenance) and all pressure and incision points were infiltrated with local anesthetic lidocaine. Once under the surgical plane of anesthesia, animals were transferred to a stereotaxic frame with body temperature constantly monitored and maintained at 37ºC by means of a thermal blanket. A craniotomy and durotomy were performed on the left or right hemisphere in order to record with epicortical or intracortical arrays, respectively. Additionally, a craniotomy and durotomy were performed over the prefrontal cortex to topically administer 5 mM KCl to induce cortical spreading depression. The large craniotomy was centred at 43 mm anterio-posterior (AP) and 42.5 mm medio-lateral (ML) and was 6 mm AP by 4.5 mm ML in size while the smaller craniotomy, located at 50 mm AP and 42 ML, was 2.5 mm AP by 1.25 mm ML. A Ag/AgCl electrode pellet was inserted in temporal muscle and used as reference both for recordings and for the measurement of the transistors transfer curve. All recording probes, either gSGFETs or microelectrodes, were placed directly on the cortical surface and kept in place by adherence to the tissue (Fig. S9a-b). A custom electronic instrumentation was used (Fig. S10), which provides the current-to-voltage conversion and the bias control for each channel. The instrumentation splits the recorded signals into two bands with different gains: low-pass filtered (< 0.16 Hz, 10^4 gain) and band-pass filtered (0.16 Hz $< f < 160$ kHz, 10^6 gain). In the experiments where only the gSGFET array was measured the low-pass filtered signals and bias control was managed by a data acquisition system (National Instruments USB-6353), while the band-pass filtered signals were directly acquired by a commercial electrophysiological recording system consisting of a programmable gain amplifier (Multichannel Systems, GmbH) and digitizer interface (CED 1401 and Spike2 software, Cambrigde Electronic Design, UK). The LPF and BPF bands were sampled at 1 Hz and 5 kHz respectively. Prior to the beginning of the recordings, the transfer curve of the gSGFET was measured *in situ* to determine the optimum bias point, generally around -0.1 V of the CNP (Fig. S9c-d).

For gSGFETs comparison experiments with microelectrodes and the glass micropipettes with Ag/AgCl wire(≈0.15 MΩ) a total of four subjects was used: two subjects were measured with gSGFETs, microelectrodes and a micropipette, one with gSGFETs and microlectrodes (data from Fig.3) and another one with gSGFETs and a micropipette (data from Fig. 2e, and Fig.S2). A custom Simulink model was used to simultaneously measure graphene transistors through an adapted g.HIamp biosignal amplifier(g.tec medical engineering GmbH, Austria) while microelectrodes and the solution-filled glass micropipette were recorded using an g.USBamp (g.tec medical engineering GmbH, Austria). The same reference electrode was used by both amplifiers and signals were sampled at 4.8 kHz.

Laser speckle contrast imaging

For the measurement of the regional cerebral blood flow (rCBF), a laser speckle contrast imaging (LSCI) system was used which consists of a continuous-wave temperature-controlled laser diode (785 nm, Thorlabs, Germany) for homogenous full-field illumination and a charge-coupled device camera (sc640-120fm, Basler, Germany), with an exposure time of 5 ms, which captures the diffused light scattered from the imaging area. The speckle contrast was calculated for the predefined region of interest (ROI) at each pixel in temporal domain over 100 frames, to ensure good signal-to-noise ratio. The statistics of different noise sources[37] was accounted for when calculating the speckle contrast. Speckle contrast was then related to a rCBF index (BF) as reported in [38,48]. Finally, the relative blood flow (ΔrCBF) was calculated as:

$$\Delta rCBF = \frac{BF - BF_B}{BF_B} * 100\ [\%]$$

where BF_Bcorresponds to the basal regional blood flow. Fig. S11 shows the area where LSCI was measured in Fig. 5c.

Data Analysis

All data were analyzed using Python 2.7 packages (Matplotlib, Numpy and Neo) and the custom library PhyREC. The conversion of the recorded current signals (LPF and BPF) to a voltage signal was performed by summation of both signals and interpolation in the *in vivo* measured transfer curve of the corresponding gSGFET. The transfer curve was always measured, at least, at the beginning and end of every acute experiment, and generally some more transfer curves measurements were performed along the duration of the experiment. Comparison of the evolution of the in vivo measured transfer curves was systematically performed during data analysis (see Fig. S12a) to ensure that no significant variations are present and to detect (if there are) any misbehaving transistor. Moreover, all recordings presented in the manuscript have been calibrated with the nearest transfer curve measured (following the procedure shown in Fig. S1) to ensure high fidelity in the voltage-converted signals. For visualization purposes microelectrode recordings were filtered (band-stop, 48-52 Hz) and down sampled at 300Hz. For the propagation analysis, the baseline of the signal was estimated as the mean value of the signal until the positive deflection. We defined the onset of the CSD as the onset of the negative shift and detected it using a threshold (Fig. S13a). We defined the WaveTime of each wave as the mean time of the triggers detected in the 16 transistors and constructed a TimeLagMatrix containing time lags for each channel computed with respect to the WaveTime (Fig. S13c). We interpolated the known time lags with a thin-plate smoothing spline technique (Fig.5a). The velocity of the propagation has been estimated computing the gradient of the TimeLagMatrix on the grid[43]. To determine the direction of the waves, a vector starting at the point with higher negative delay (leader of the propagation) and pointing to the one with the highest positive delay (follower of the propagation) was transformed into polar coordinates to obtain the angle (Fig. S13b). For the colormaps of Fig. 5b,c and Fig. 6b a bicubic interpolation was perfomed for visualization purposes.

Reference electrode

Voltages at drain and source terminals used to operate graphene transistors are referred to the reference electrode. The reference electrode is generally grounded in anaesthetized subjects to ensure stable recordings, since the subject is grounded at many points. However, the requirement of the reference electrode to be grounded is not necessary; provided that the reference electrode is properly positioned in a non-active location and does not have drifts and oscillations that interfere with the recording, a proper operation of the graphene transistor is achieved. Importantly, gSGFETs are less sensitive than microelectrode technology to the baseline drift associated with the reference electrode.

Commonly, baseline drift can lead to saturation of the amplifiers used for microelectrode DC-coupled recordings, while the operation principle of graphene transistors does not lead to saturation. The drift of the reference electrode shifts the biasing point which could lead to non-optimal performance of gSGFETs. However, this can be easily solved by changing the transistor bias to the new optimal value, which can be obtained from measuring an in vivo transfer curve.

Code Availability

Custom code developed for neurophysiological analysis of gSGFET signals is available at: https://github.com/aguimera/PhyREC.

Data Availability

The experimental data that support the figures within this paper and other findings of this study can be accessed by contacting the corresponding authors. Authors can make data available on request, agreeing on data formats needed.

Methods References

37 Valdes, C. P. *et al.* Speckle contrast optical spectroscopy, a non-invasive, diffuse optical method for measuring microvascular blood flow in tissue. *Biomedical optics express* **5**, 2769-2784 (2014).

38 Boas, D. A. & Dunn, A. K. Laser speckle contrast imaging in biomedical optics. *Journal of biomedical optics* **15**, 011109 (2010).

43 Capone, C. *et al.* Slow Waves in Cortical Slices: How Spontaneous Activity is Shaped by Laminar Structure. *Cerebral Cortex*, 1-17 (2017).

46 de la Rosa, C. J. L. *et al.* Frame assisted H[sub 2]O electrolysis induced H[sub 2] bubbling transfer of large area graphene grown by chemical vapor deposition on Cu. *Applied Physics Letters* **102**, 022101-022104 (2013).

47 Illa, X., Rebollo, B., Gabriel, G., Sánchez-Vives, M. V. & Villa, R. in *SPIE Microtechnologies.* 951803-951803-951806 (International Society for Optics and Photonics).

48 Bandyopadhyay, R., Gittings, A., Suh, S., Dixon, P. & Durian, D. J. Speckle-visibility spectroscopy: A tool to study time-varying dynamics. *Review of scientific instruments* **76**, 093110 (2005).